NASA TM X-779

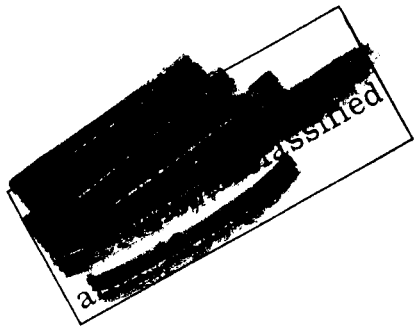

TECHNICAL MEMORANDUM

X-779

THE EFFECTS OF NOSE BLUNTNESS ON THE PRESSURE FLUCTUATIONS MEASURED ON 15° AND 20° CONE-CYLINDERS AT TRANSONIC SPEEDS

By Charles F. Coe and Arthur J. Kaskey

Ames Research Center
Moffett Field, Calif.

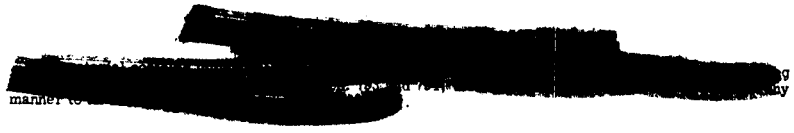

NATIONAL AERONAUTICS AND SPACE ADMINISTRATION
WASHINGTON

January 1963

[redacted]

NATIONAL AERONAUTICS AND SPACE ADMINISTRATION

TECHNICAL MEMORANDUM X-779

THE EFFECTS OF NOSE BLUNTNESS ON THE PRESSURE FLUCTUATIONS MEASURED ON 15° AND 20° CONE-CYLINDERS AT TRANSONIC SPEEDS*

By Charles F. Coe and Arthur J. Kaskey

SUMMARY

Pressure fluctuations have been measured along the top center lines of seven cylindrical bodies having noses with 15° and 20° cone-cylinder intersection angles and various amounts of hemispherical bluntness. A hemisphere cylinder was also tested. Tests were conducted at angles of attack of 0°, 4°, and 8° over a Mach number range within 0.60 to 1.17.

The results of the investigation showed that pressure fluctuations in regions of separated flow or at the locations of shock waves were smaller on cylindrical bodies with 15° cone-cylinder intersection angles than with 20° intersection angles. Hemispherical blunting of the nose cones had little or no effect on the pressure fluctuations. Replacing the 15° or 20° half-angle cones with a hemisphere, however, resulted in increased fluctuations due to separation.

INTRODUCTION

Since the trend of shapes in space vehicle windshields has been toward hemisphere-cone noses and other combinations of cones and cylinders for the rocket stages, research was undertaken to investigate the limits of cone angles and cone bluntness that could be used without introducing fluctuations due to separation. Tests of an early configuration of the Nimbus-EGO satellite shroud with a blunted cone nose and a 20° cone-cylinder intersection angle served as a starting point in the present investigation since separation effects were noticeable in the results. The progression of nose profiles proceeded to less bluntness of the 20° nose and then to a pointed 15° half-angle cone nose which was expected to show favorable characteristics in view of the Centaur model results in reference 1. Three models having 15° half-angle cone noses with different amounts of hemispherical blunting and a model with a hemispherical nose were also tested.

*Title, Unclassified

The root mean square of the pressure fluctuations measured along the top center lines of the models are presented in the report. These tests were conducte as part of a research program at Ames Research Center to investigate both the over all buffet loads and local steady and fluctuating pressures at transonic speeds on various body shapes. Other results from this investigation are in references 1, 2 and 3.

NOTATION

$\Delta C_p(RMS)$	coefficient of the root-mean-square fluctuations of pressure about the mean $\frac{\Delta p(RMS)}{q_o}$
M	free-stream Mach number
Re	Reynolds number
D	maximum body diameter
H	height of pointed nose cone
$\Delta p(RMS)$	root-mean-square fluctuations of pressure about the mean
q_o	free-stream dynamic pressure
h	height of blunted nose cone
x	distance along body axis from cone-cylinder intersection
α	angle of attack

APPARATUS AND TECHNIQUE

Models

Sketches of the seven models that were tested are shown in figure 1, along with the pertinent dimensions. The locations of the pressure transducers as tabulated in figure 1 were slightly different on the models labeled B from those on the models labeled A. All of the models had cylindrical bodies with the same length and diameter except for the model with the blunted 20^o half-angle cone nose. On this model, the cylindrical section was shorter and had a sharp step that reduced the diameter from 9.125 to 8.4 inches at approximately the midpoint of the cylinder. It should be noted that all the transducers were located forward of the step and, in addition, on this particular model, the transducer on the cone at station -0.2 was omitted.

The models, which were considered to be rigid, were constructed of wood and glass fiber supported with steel rings. Shake tests to determine the resonant frequencies of the combined model and support system were not performed. However, the system was similar to that presented in reference 1, for which the effects of motion were small.

Wind Tunnel and Instrumentation

Tests were conducted in the Ames 14-Foot Transonic Wind Tunnel within a Mach number range of 0.60 to 1.17. Reynolds number varied with Mach number as illustrated by the shaded band in figure 2.

The pressure transducers and electronic components used for recording the pressure fluctuations were the same as in reference 1, with the exception of the revised band-pass filtering described in reference 3 which was used for the root-mean-square measurements. Figure 3 shows the amplitude response through the applied filtering. The 0.250-inch-diameter transducers were flush mounted. The back side of the diaphragm of each transducer was referenced to the time-average static pressure from an adjacent orifice so that the transducers responded only to the fluctuations of pressure about the mean. A steady reference pressure was insured by using approximately 150 feet of tubing to connect the transducer and its adjacent orifice.

Procedure

The calibration and data reduction methods were the same as those described in reference 1. The tests were conducted at constant angles of attack of 0°, 4°, and 8° over a range of Mach numbers which varied somewhat for the different models, but which had as its limits $M = 0.6$ to $M = 1.17$. In the range of Mach numbers where significant pressure fluctuations occurred in the regions of the normal shock waves ($0.7 < M < 0.95$), the Mach number was adjusted in whatever increments were required to locate the maximum intensities at successive pressure transducer stations.

RESULTS AND DISCUSSION

The longitudinal distributions of the pressure fluctuations as measured along the top center lines of each of the models are in figures 4 through 10. For convenience in comparing fluctuations on the models, representative distributions of the fluctuations for the two cone angles and their limits of bluntness are shown for each angle of attack in figure 11. When the fluctuations are discussed, reference is made to fluctuations that occur in the regions of normal shock waves and also to fluctuations that occur in regions of separated flow. As previously noted in references 1 and 2, the fluctuations in the regions of the shock wave are characterized by locally concentrated peaks, while the fluctuations in separated flows, although of lower amplitude, occur over larger areas.

Effect of Cone-Cylinder Intersection Angle

Comparison of the pressure fluctuations on the models having 15° and 20° cone-cylinder intersection angles (figs. 4, 6, and 11) shows that the fluctuations in either the regions of the shock waves or separated flows were smaller on the models with 15° corner angles. Fluctuations behind the shock wave occurred on the model with the 20° corner angle at angles of attack of 0°, 4°, and 8° at Mach numbers from 0.74 to 1.00. These fluctuations, plus the higher fluctuations in the region of the shock wave, would result in higher buffeting inputs on rocket configurations having 20° cone-cylinder intersection angles than on those having 15° intersection angles. Although tests were not conducted with corner angles larger than 20°, shadowgraph pictures showing large regions of separated flow on hemisphere cone-cylinder models having corner angles of 30° and 45° appear in reference 4.

Effect of Cone Bluntness

The effects of cone bluntness can be seen by comparing the distributions of the pressure fluctuations in figures 4, 5, and 11 for the 20° cone-cylinder models and in figures 6 through 9, and 11 for the 15° cone-cylinder models. As mentioned in the Introduction, the investigation of the effects of cone bluntness started with the 20° cone-cylinder model blunted to $h/H_{20} = 0.567$. The results show that the extension of the cone to a point had little effect on the pressure fluctuations in either the regions of the shock wave or in the regions of separated flow.

The nose shapes investigated on the 15° cone-cylinder models were a pointed cone, one blunted to about the same fineness ratio as the pointed 20° half-angle cone nose, one blunted to half the height of the cone, and last, one blunted to about the same fineness ratio as the blunted 20° half-angle cone nose. It can be noted from the results that there was also little effect of the various degrees of bluntness on the 15° half-angle cone noses up to the limit of bluntness tested, $h/H_{15} = 0.424$. This conclusion was based on a comparison of data over the complete Mach number range of the tests. When the maximum fluctuations in the region of the shock wave were compared, consideration was given to the difference in transducer stations on the pointed cone model. The fact that the results were affected more by corner angle than by cone bluntness indicates that the corner angle is the more important parameter governing the flow on bodies with hemisphere-cone noses.

Tests were also conducted with a model which had a hemispherical nose. The results in figure 10 show that high-level fluctuations due to separation occurred between and including Mach numbers of 0.8 and 0.9 on the cylinder with the hemisphere nose.

A few representative shadowgraph pictures of the flow on some of the models are shown in figure 12. It is interesting to note that turbulence or separation following a shock wave was not completely eliminated on the model with the 15° hemisphere-cone nose for which the pressure fluctuations were small.

CONCLUSIONS

Measurements at transonic speeds of the fluctuating pressures along the top center lines of cylindrical bodies having nose cones with 15° and 20° cone-cylinder intersection angles and various amounts of hemispherical blunting have shown the following:

1. Pressure fluctuations which occurred in regions of separated flow or at the locations of shock waves were smaller on cylindrical bodies with 15° cone-cylinder intersection angles than with 20° intersection angles.

2. Within the limits of these tests, hemispherical blunting of the nose cones had little effect on the pressure fluctuations.

3. Replacing the blunted 15° and 20° half-angle cones with a hemisphere resulted in increased fluctuations due to separation.

Ames Research Center
National Aeronautics and Space Administration
Moffett Field, Calif., Sept. 17, 1962

REFERENCES

1. Coe, Charles F.: Steady and Fluctuating Pressures at Transonic Speeds on Two Space-Vehicle Payload Shapes. NASA TM X-503, 1961.

2. Coe, Charles F.: The Effects of Some Variations in Launch-Vehicle Nose Shape on Steady and Fluctuating Pressures at Transonic Speeds. NASA TM X-646, 1962.

3. Coe, Charles F., and Nute, James B.: Steady and Fluctuating Pressures at Transonic Speeds on Hammerhead Launch Vehicles. NASA TM X-778, 1962.

4. Treon, Stuart L.: Effects of Nose-Cone Angle on the Transonic Aerodynamic Characteristics of a Blunt Cone-Cylinder Body Having a Cylindrical, Flared, or Blunt-Finned Afterbody. NASA TM X-582, 1961.

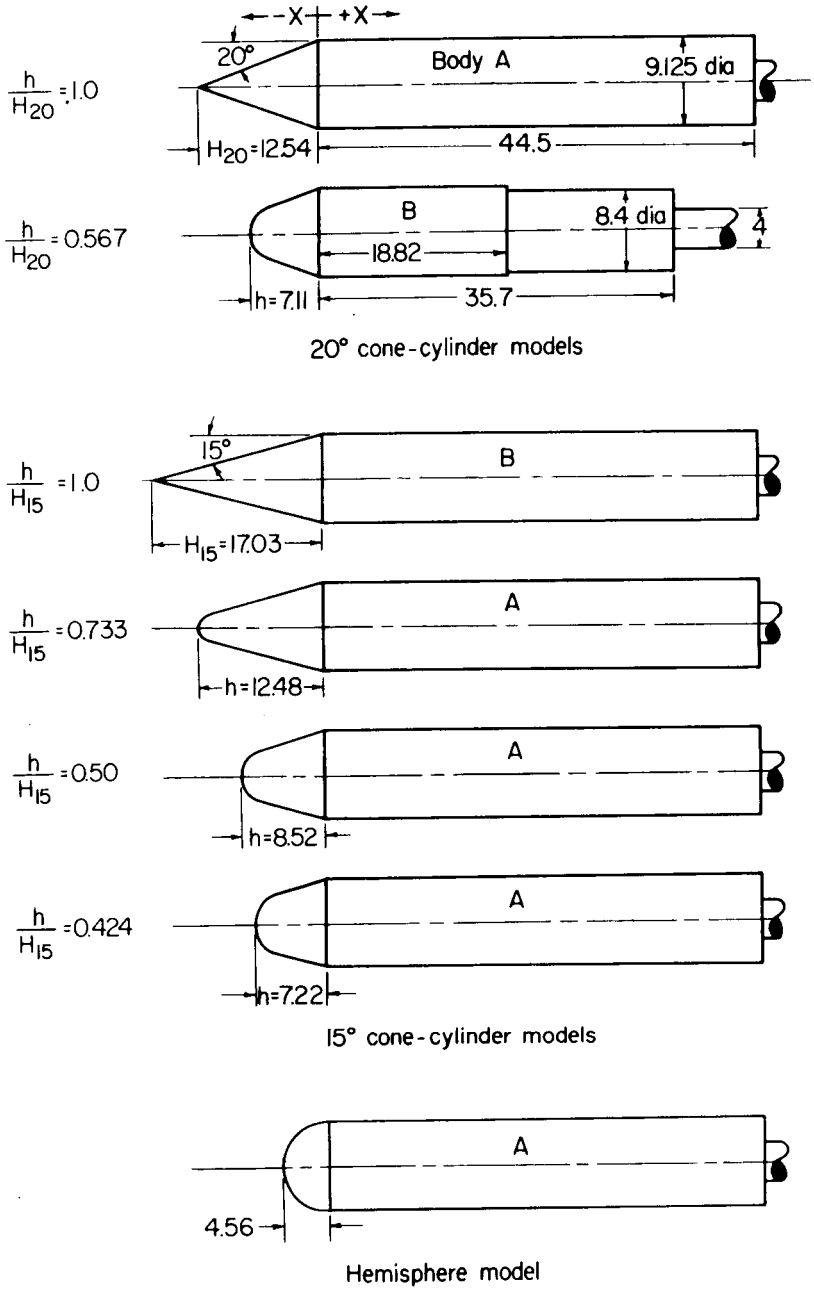

NOTE: All dimensions in inches

PRESSURE TRANSDUCER LOCATIONS $X/_D$		
	BODY A	BODY B
1	-.116	-.200
2	.038	.073
3	.158	.164
4	.300	.255
5	.500	.409
6	.700	.646
7	.900	.865
8	1.100	1.084
9	1.300	1.304
10	1.500	1.521
11	1.700	1.742
12	1.900	
13	2.100	

Figure 1.- Profiles of models.

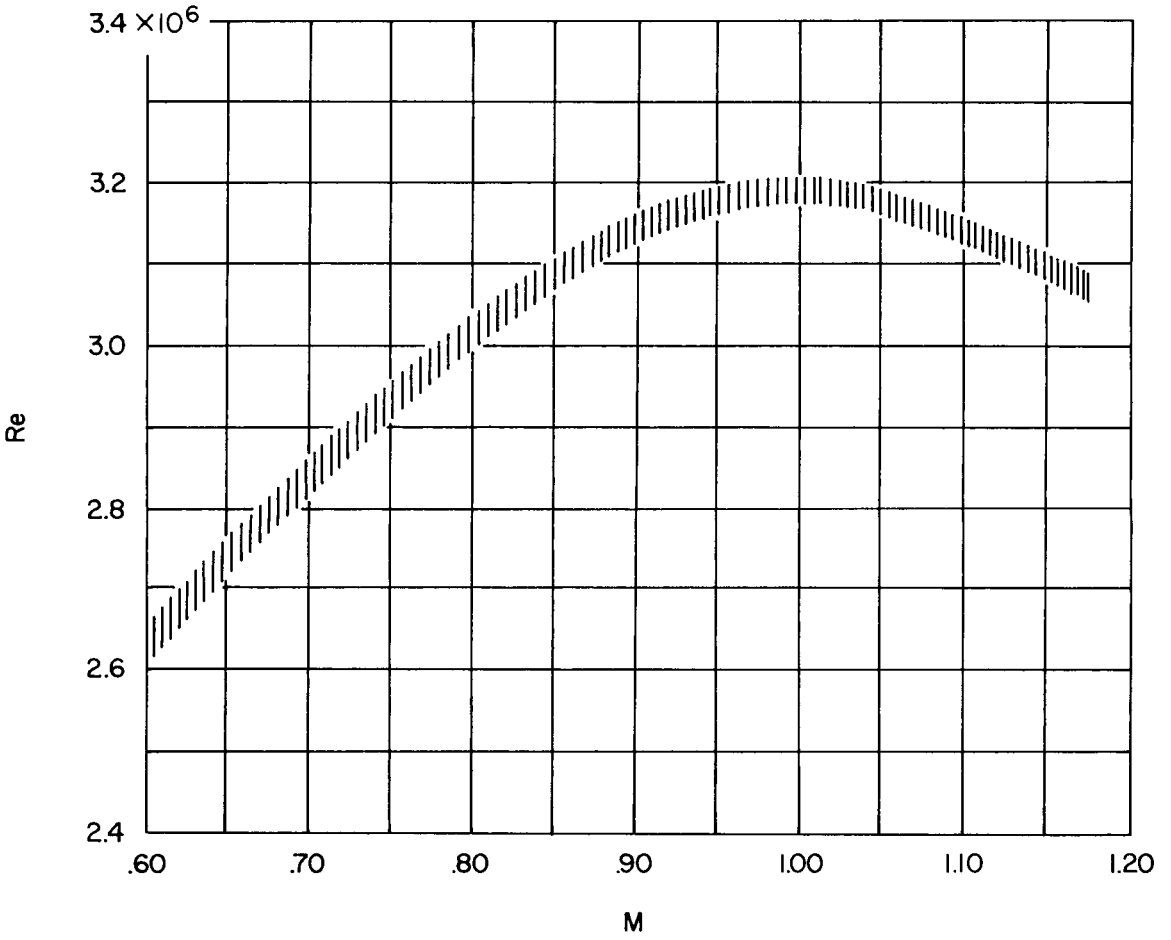

Figure 2.- Reynolds number range of the tests.

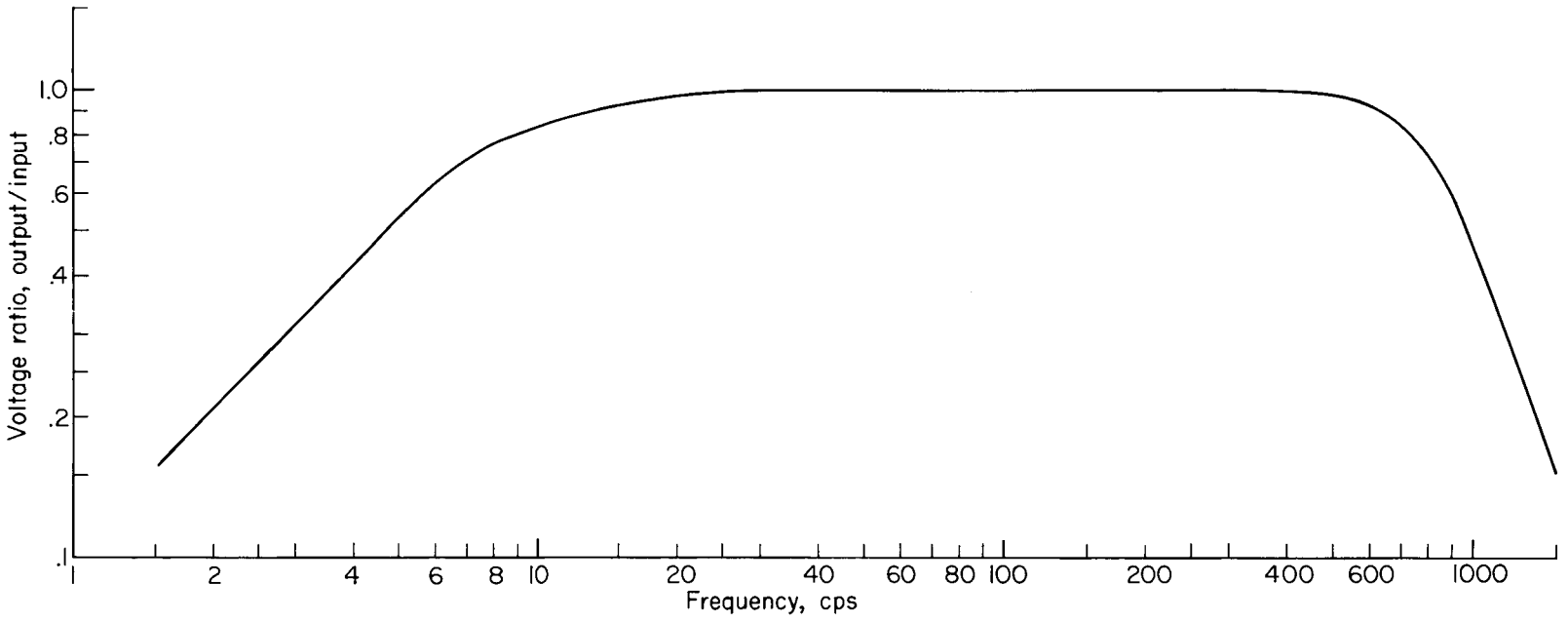

Figure 3.- Amplitude response curve showing the filtering applied to the root-mean-square measurements.

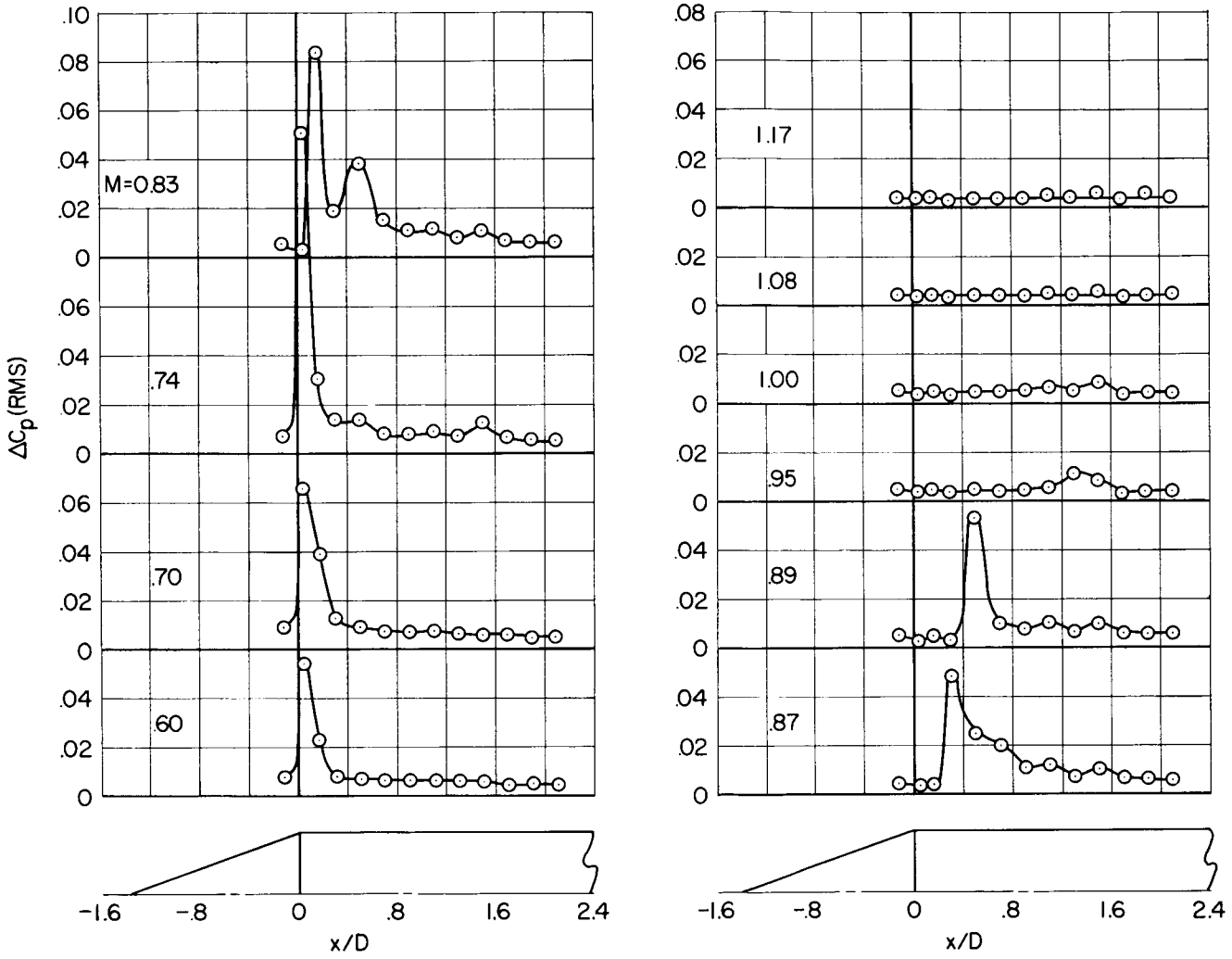

(a) $\alpha = 0^{\circ}$

Figure 4.- Pressure fluctuations on the 20° cone-cylinder model.

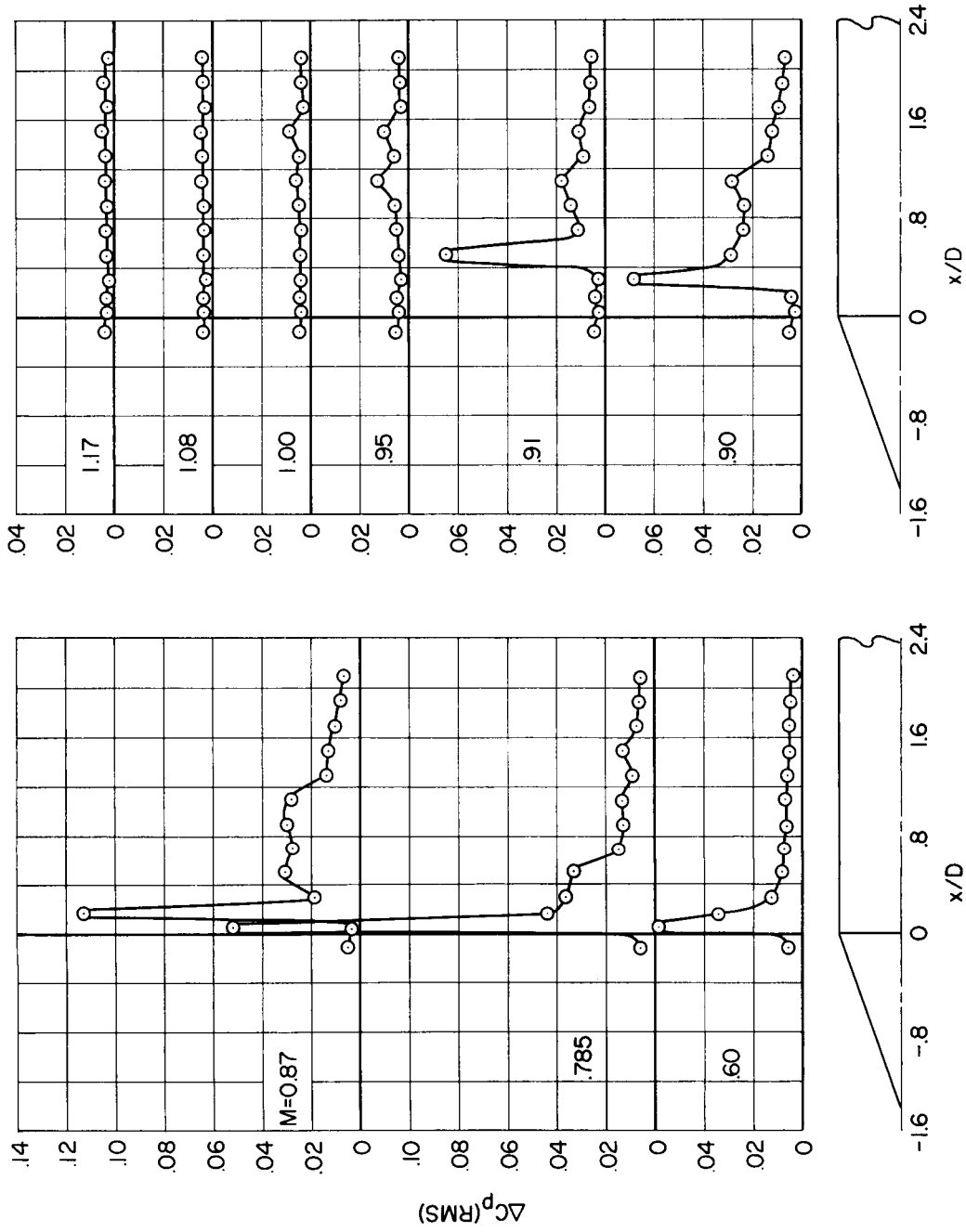

(b) $\alpha = 4^{\circ}$

Figure 4.- Continued.

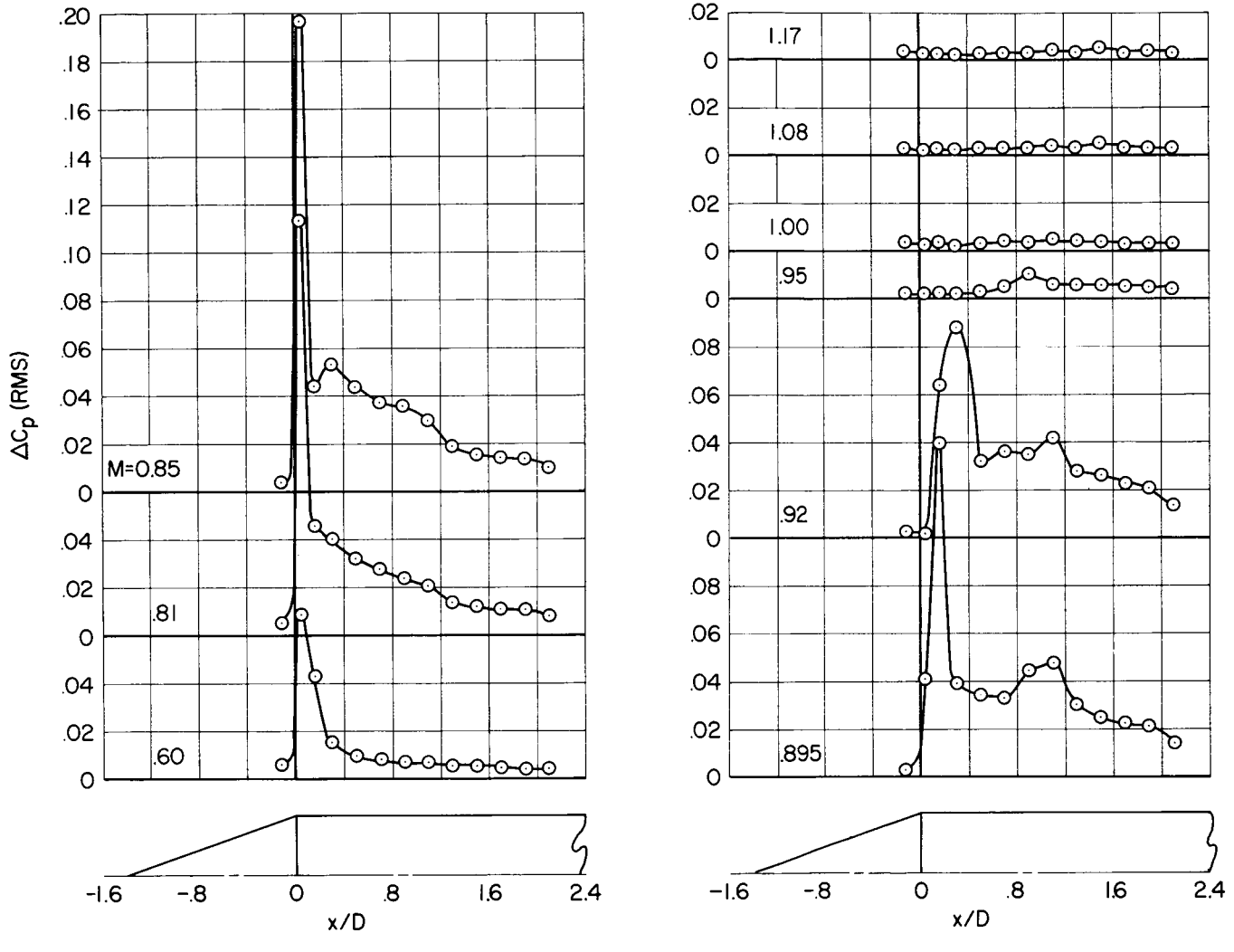

(c) $\alpha = 8^{\circ}$

Figure 4.- Concluded.

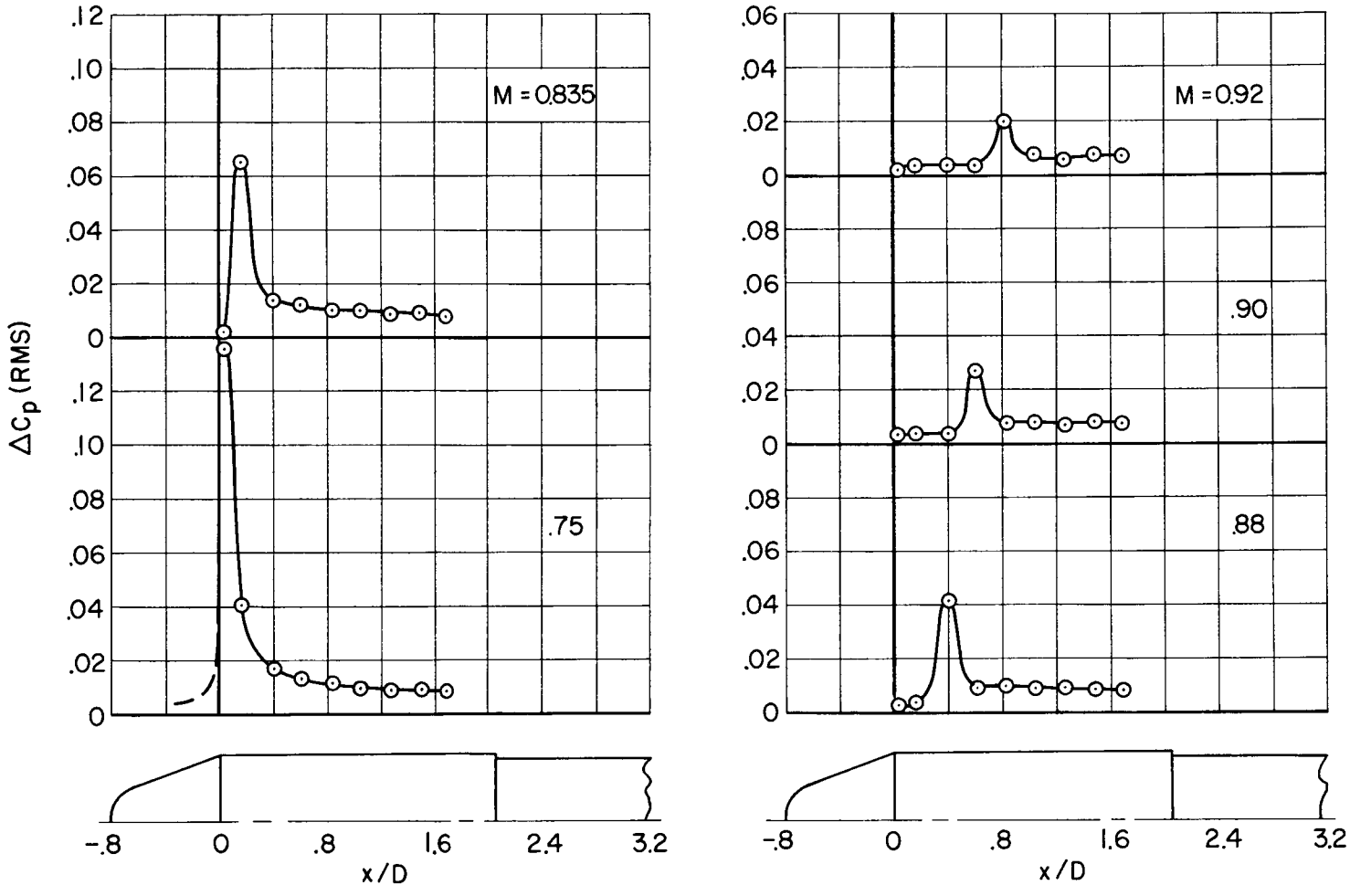

(a) $\alpha = 0^\circ$

Figure 5.- Pressure fluctuations on the 20° hemisphere cone-cylinder model blunted to $\frac{h}{H_{20}} = 0.567$.

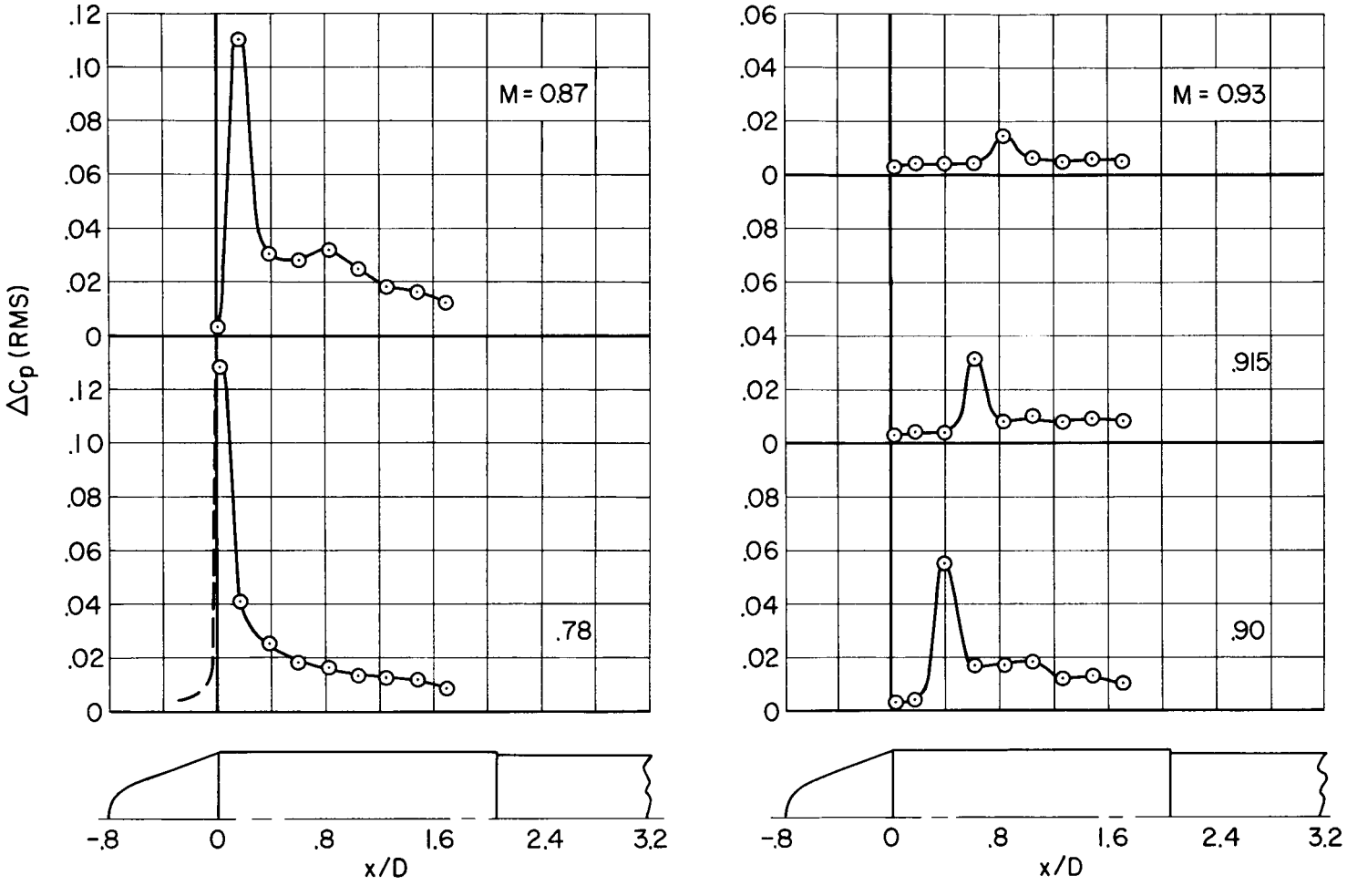

(b) $\alpha = 4^\circ$

Figure 5.- Continued.

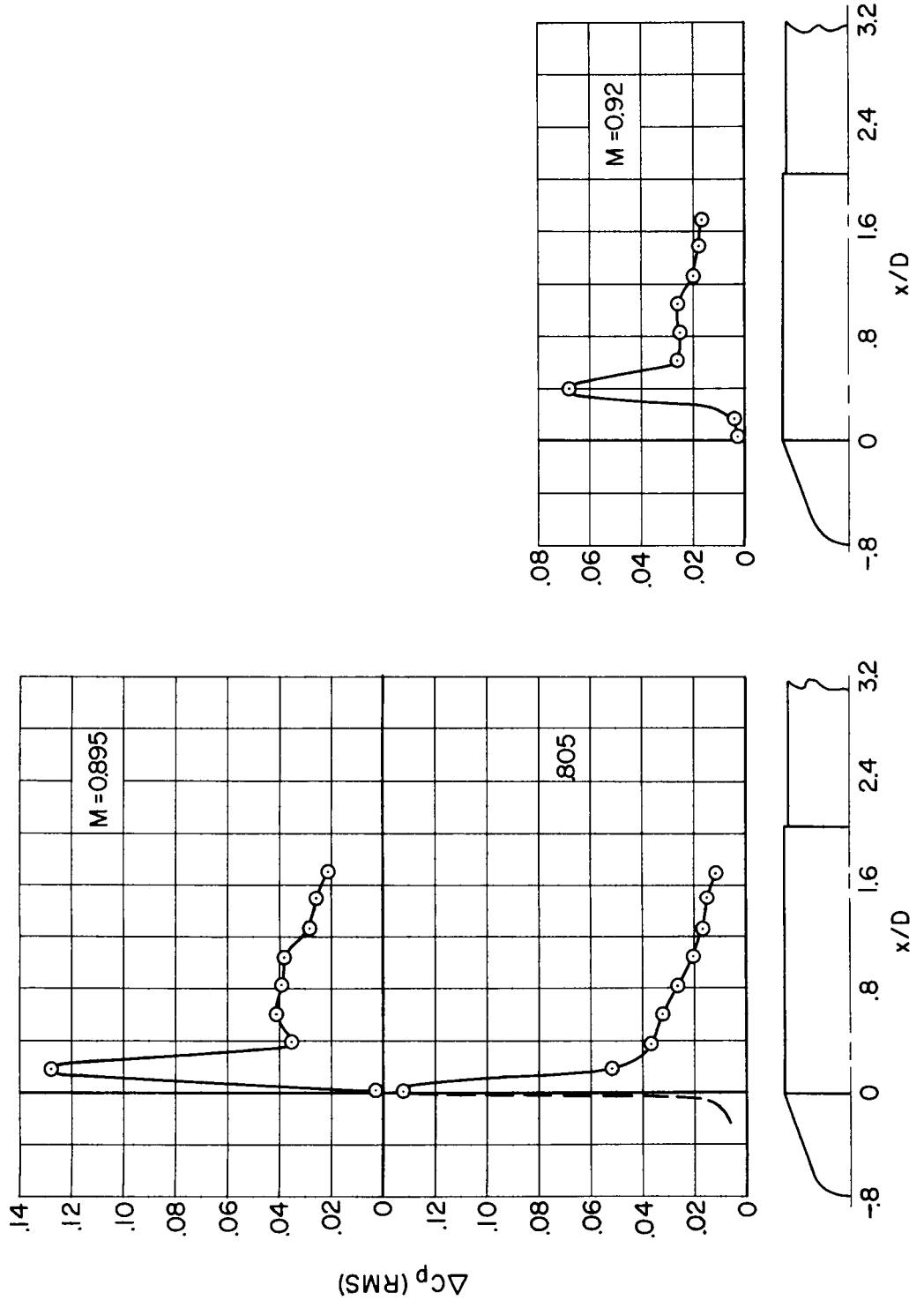

(c) $\alpha = 8^\circ$

Figure 5.- Concluded.

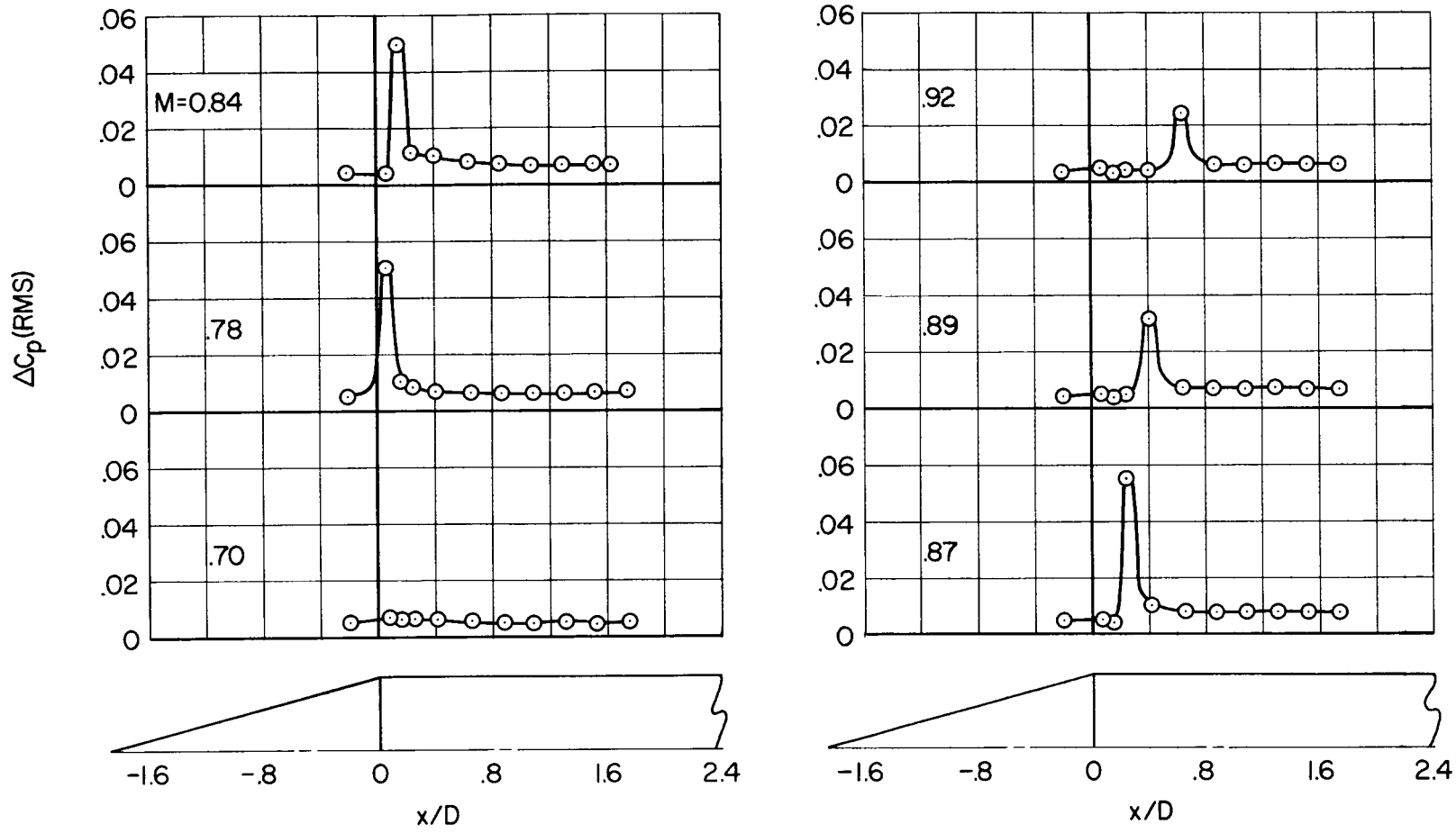

(a) $\alpha = 0^{\circ}$

Figure 6.- Pressure fluctuations on the 15° cone-cylinder model.

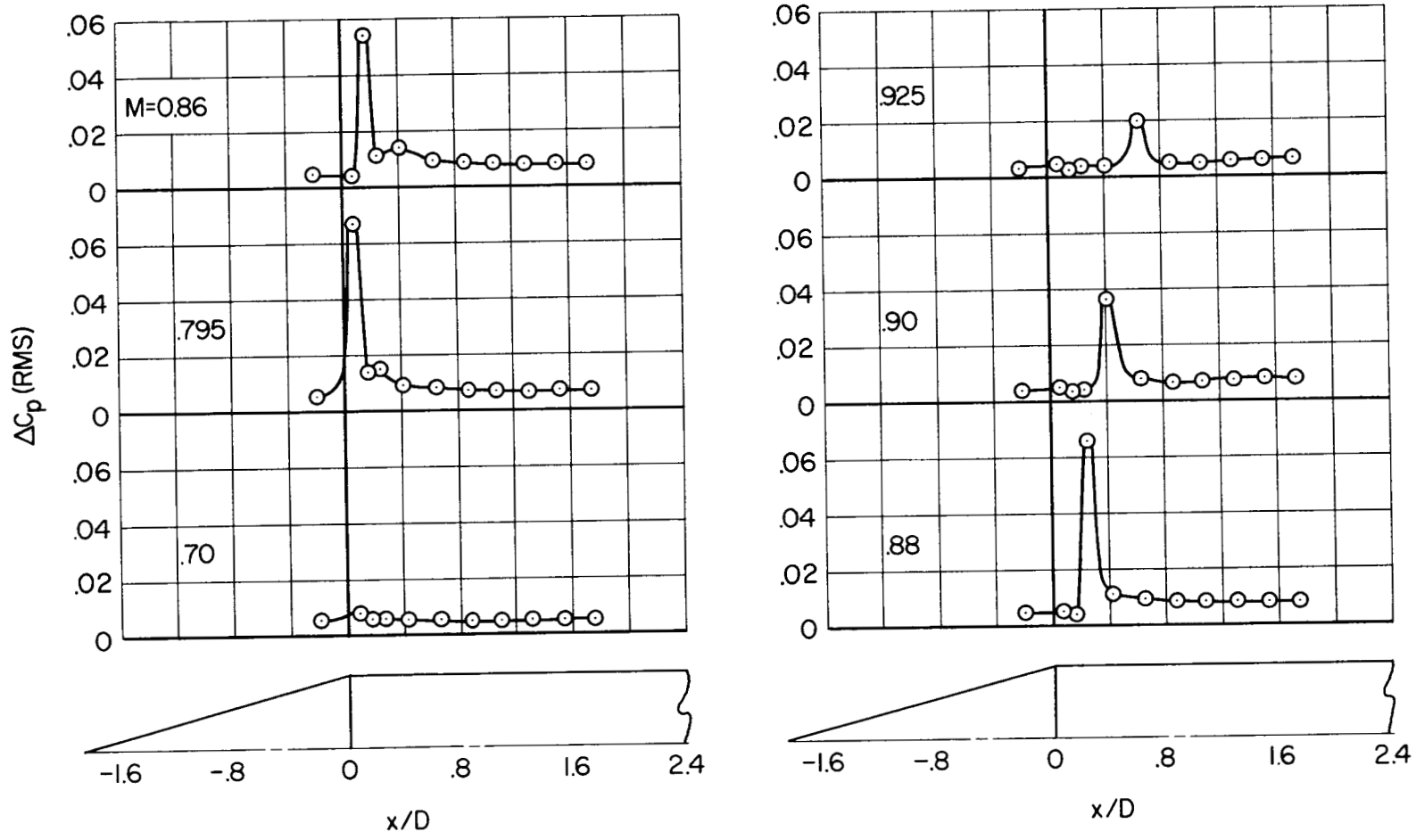

(b) $\alpha = 4^{\circ}$

Figure 6.- Continued.

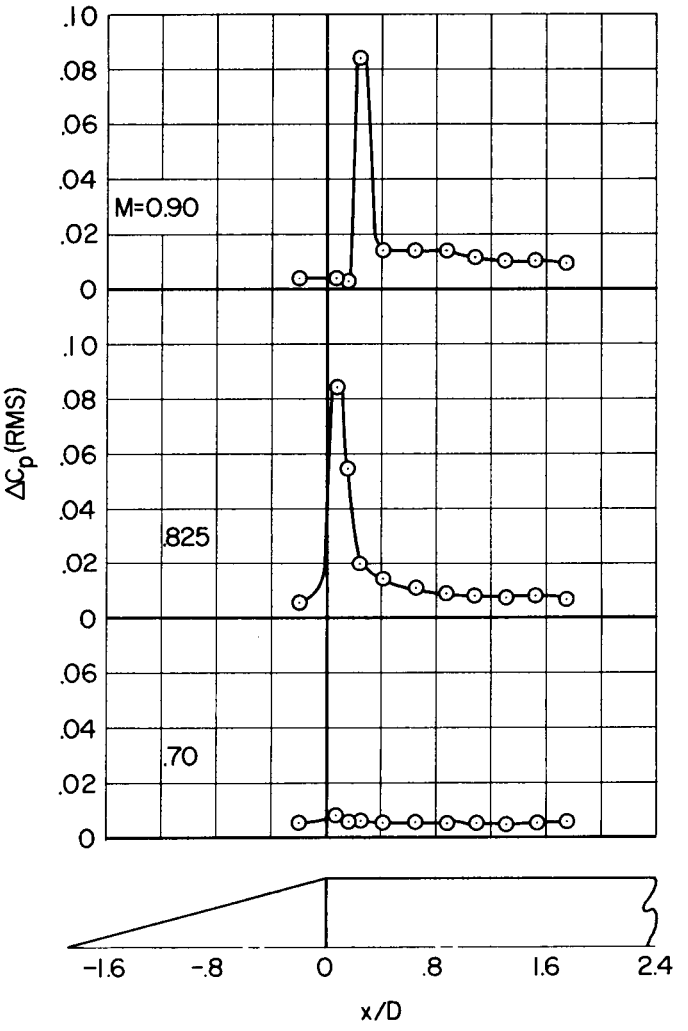

(c) $\alpha = 8^{\circ}$

Figure 6.- Concluded.

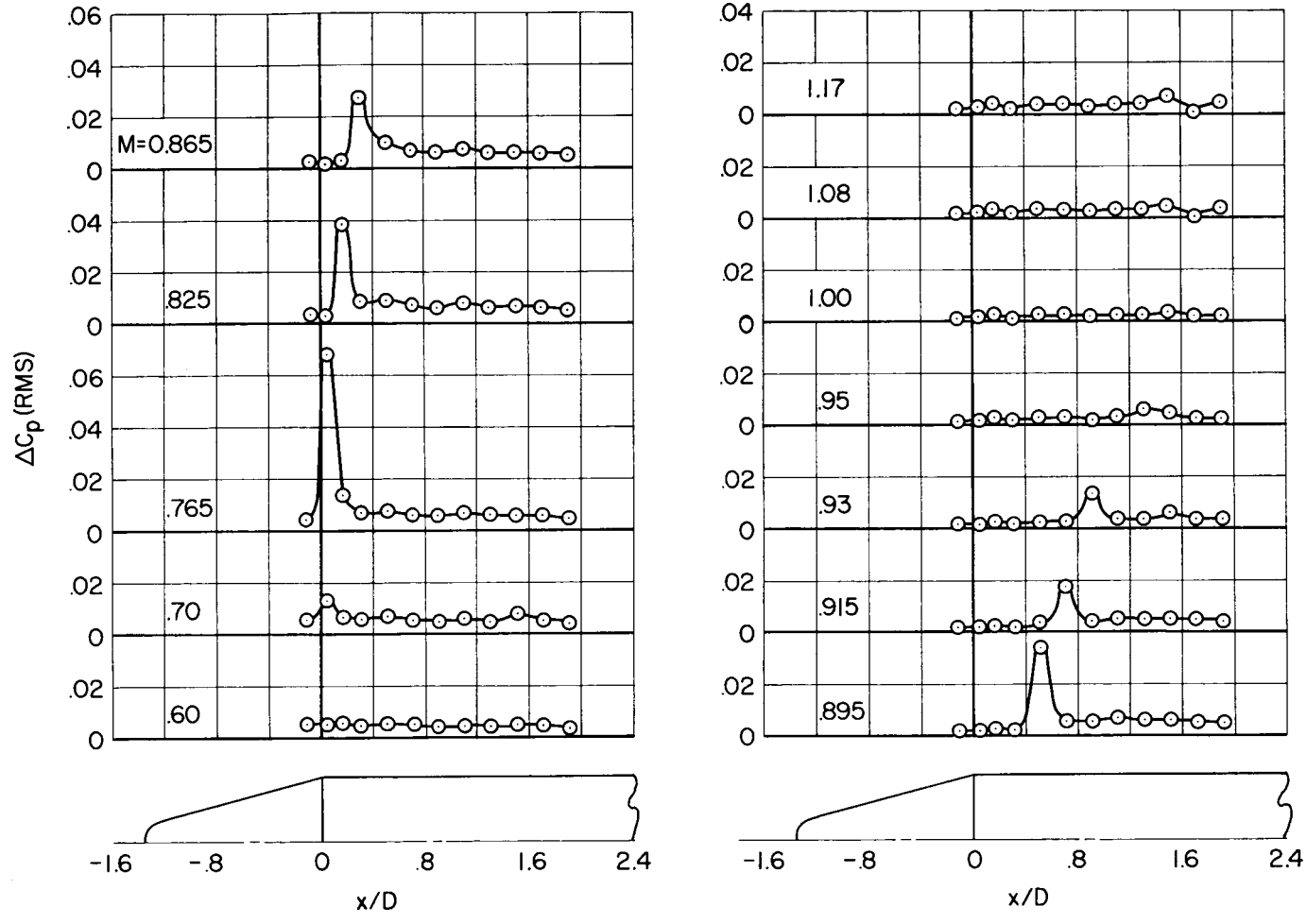

(a) $\alpha = 0^{\circ}$

Figure 7.- Pressure fluctuations on the 15° hemisphere cone-cylinder model blunted to $\frac{h}{H_{15}} = 0.733$.

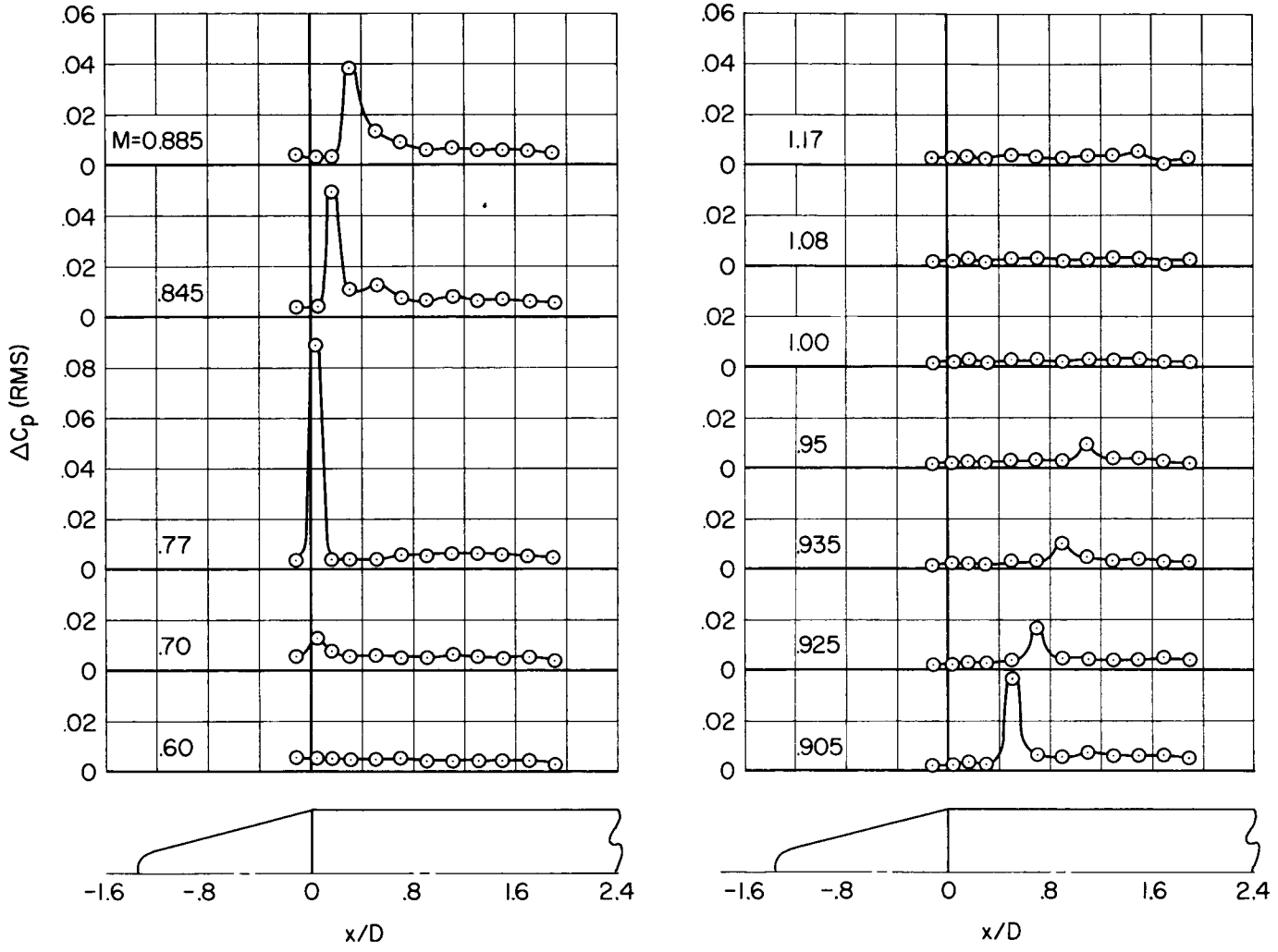

(b) $\alpha = 4^{\circ}$

Figure 7.- Continued.

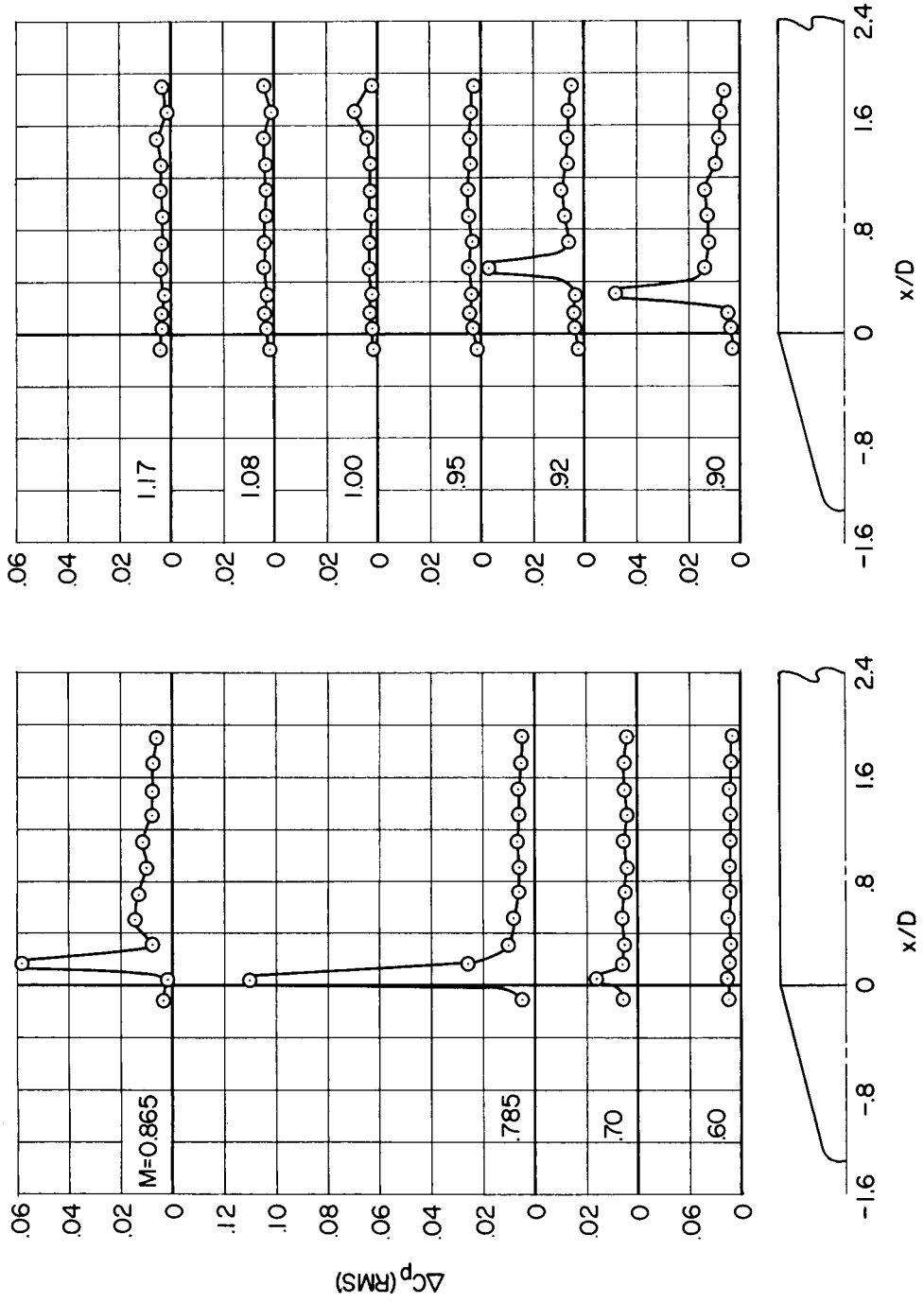

(c) $\alpha = 8^\circ$

Figure 7.- Concluded.

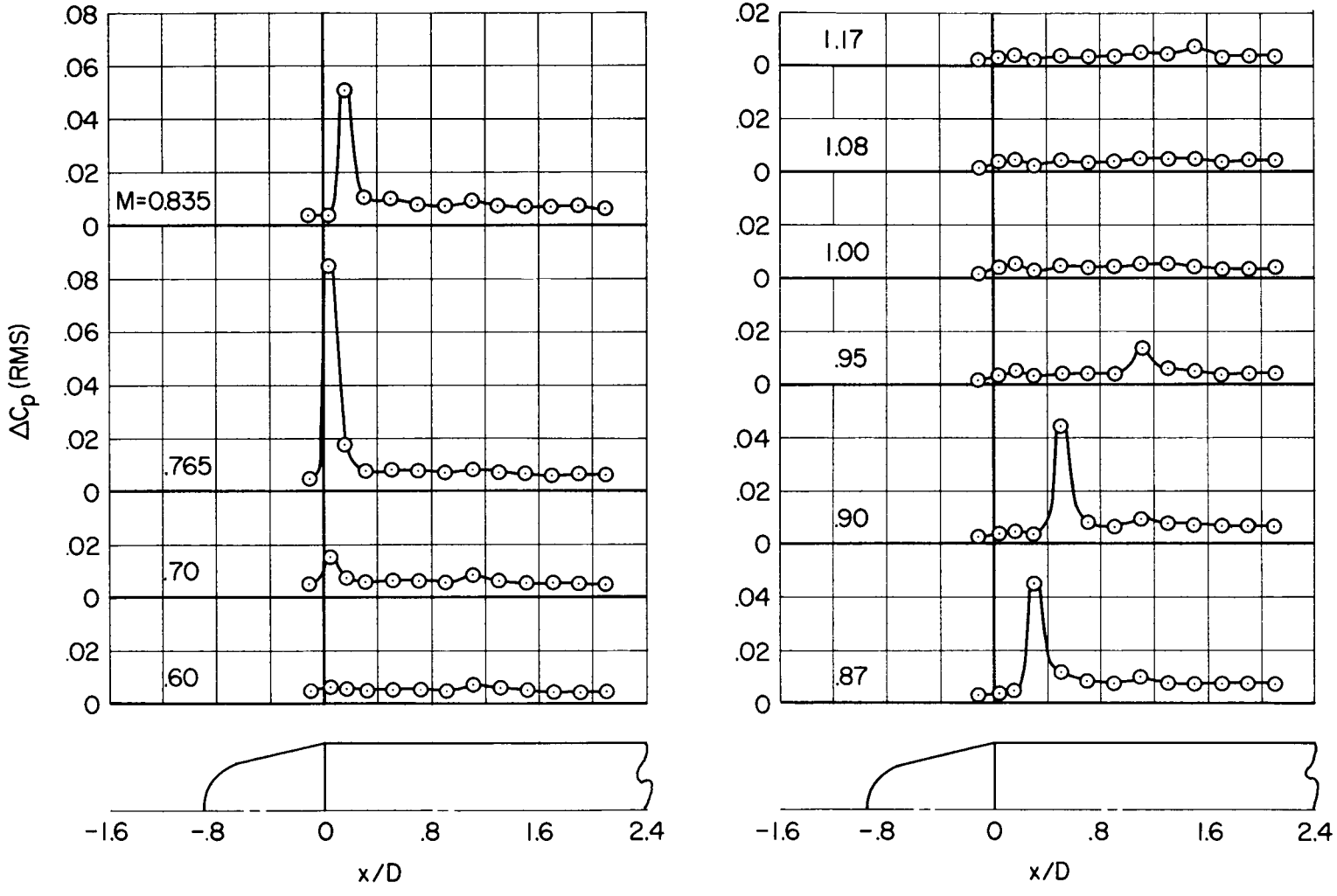

(a) $\alpha = 0^{\circ}$

Figure 8.- Pressure fluctuations on the 15° hemisphere cone-cylinder model blunted to $\frac{h}{H_{15}} = 0.50$.

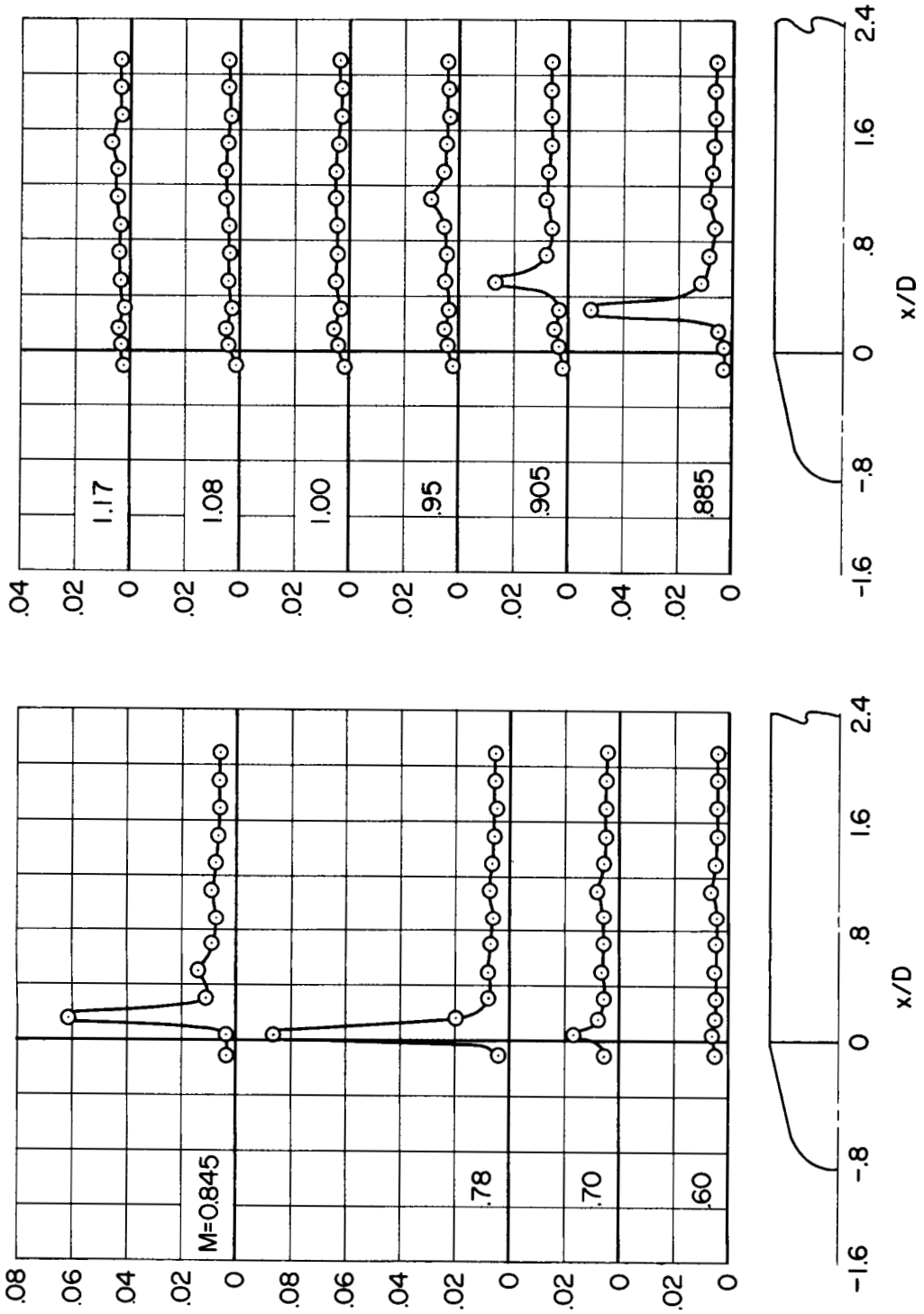

(b) $\alpha = 4^{\circ}$

Figure 8.- Continued.

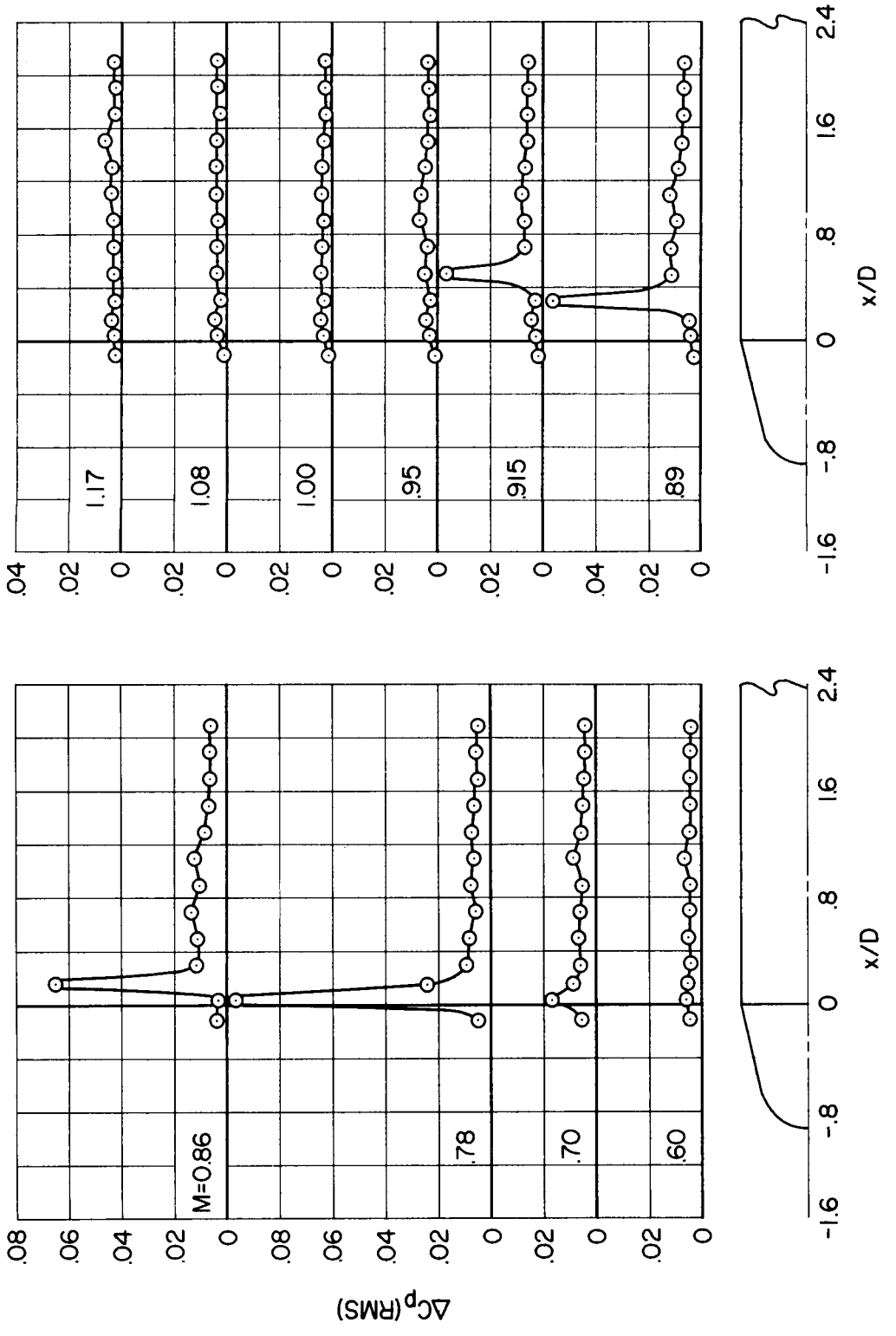

(c) $\alpha = 8^{\circ}$

Figure 8.- Concluded.

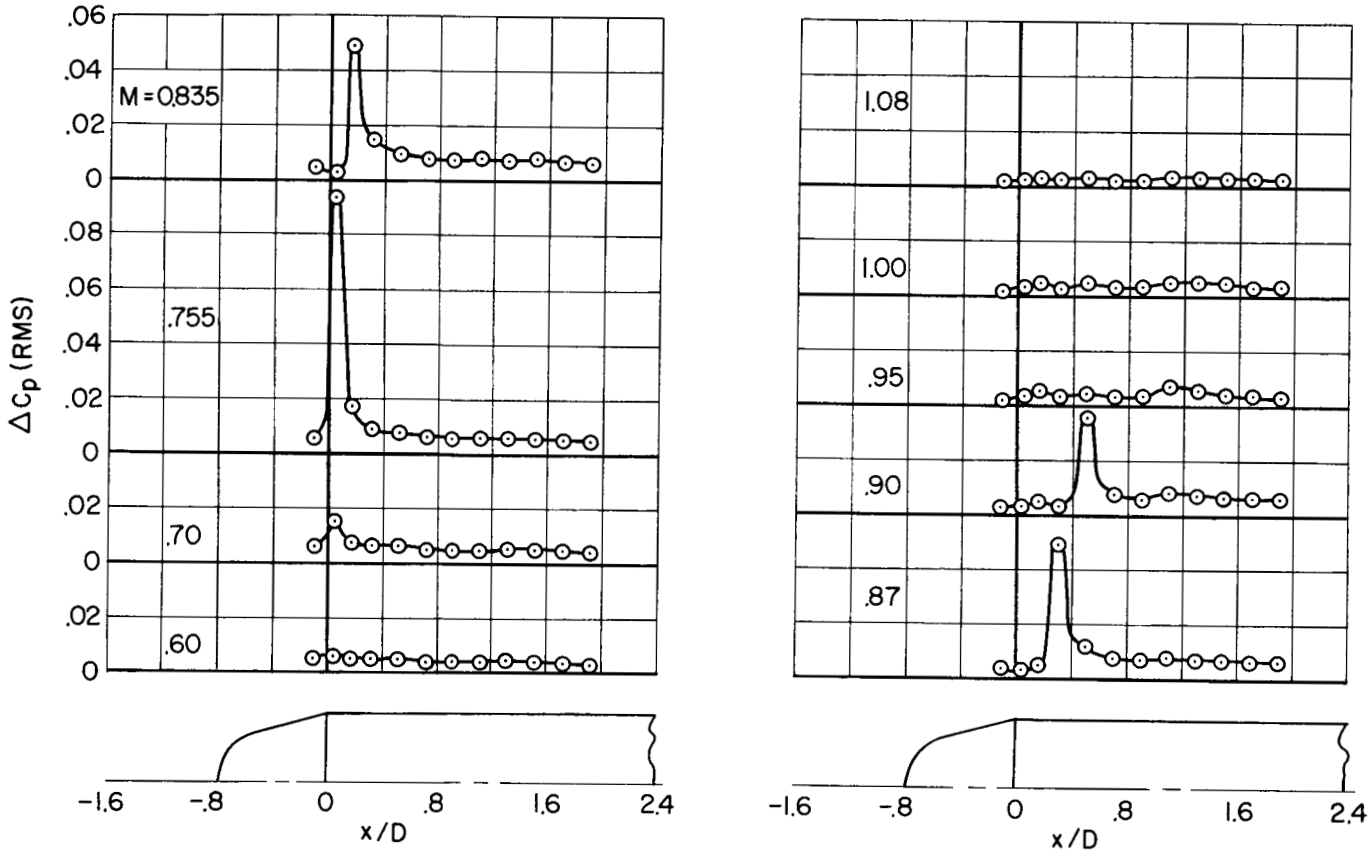

(a) $\alpha = 0^{\circ}$

Figure 9.- Pressure fluctuations on the 15° hemisphere cone-cylinder model blunted to $\frac{h}{H_{15}} = 0.424$.

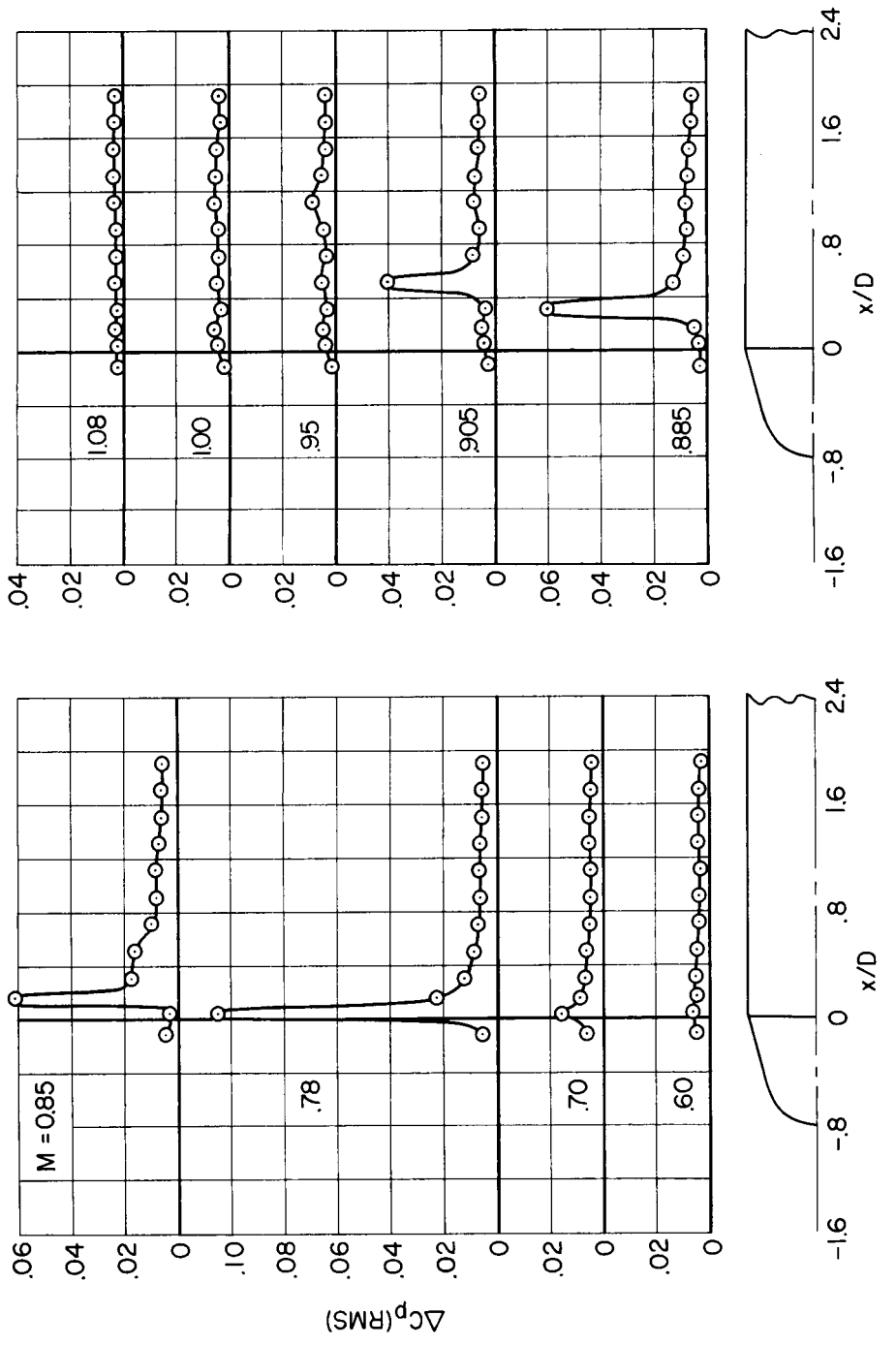

(b) $\alpha = 4^{\circ}$

Figure 9.- Continued.

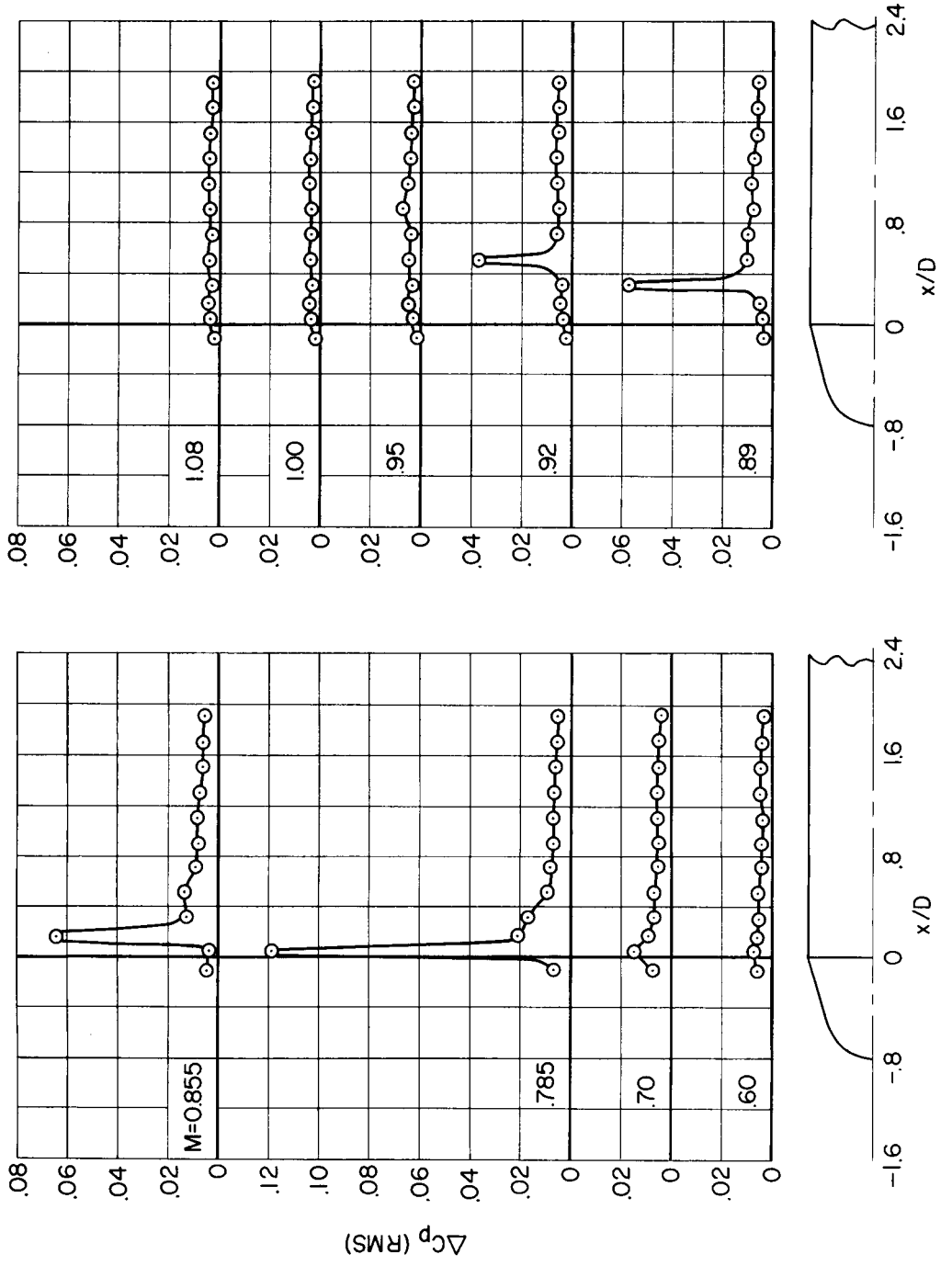

(c) $\alpha = 8^{\circ}$

Figure 9.- Concluded.

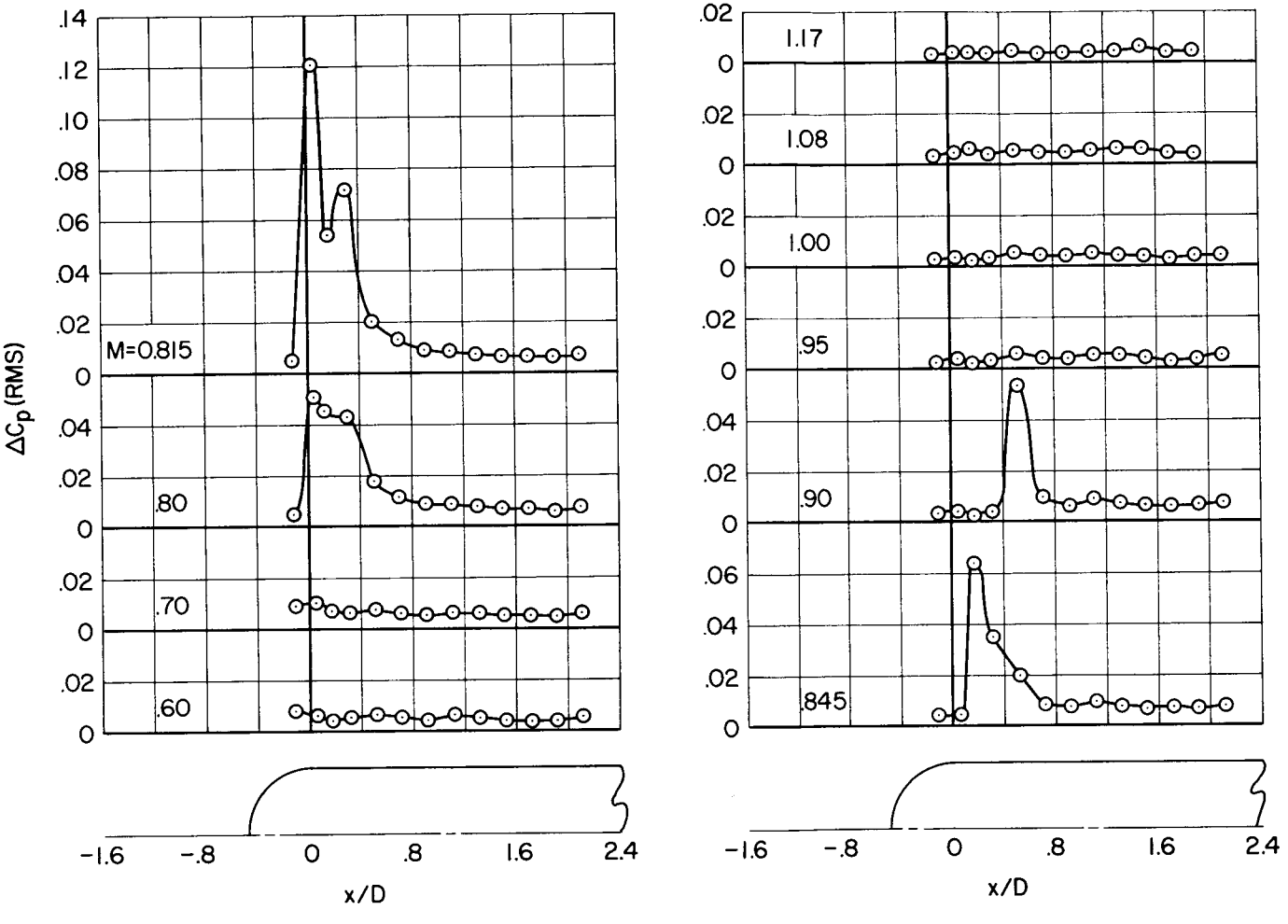

(a) $\alpha = 0^{\circ}$

Figure 10.- Pressure fluctuations on the hemisphere-cylinder model.

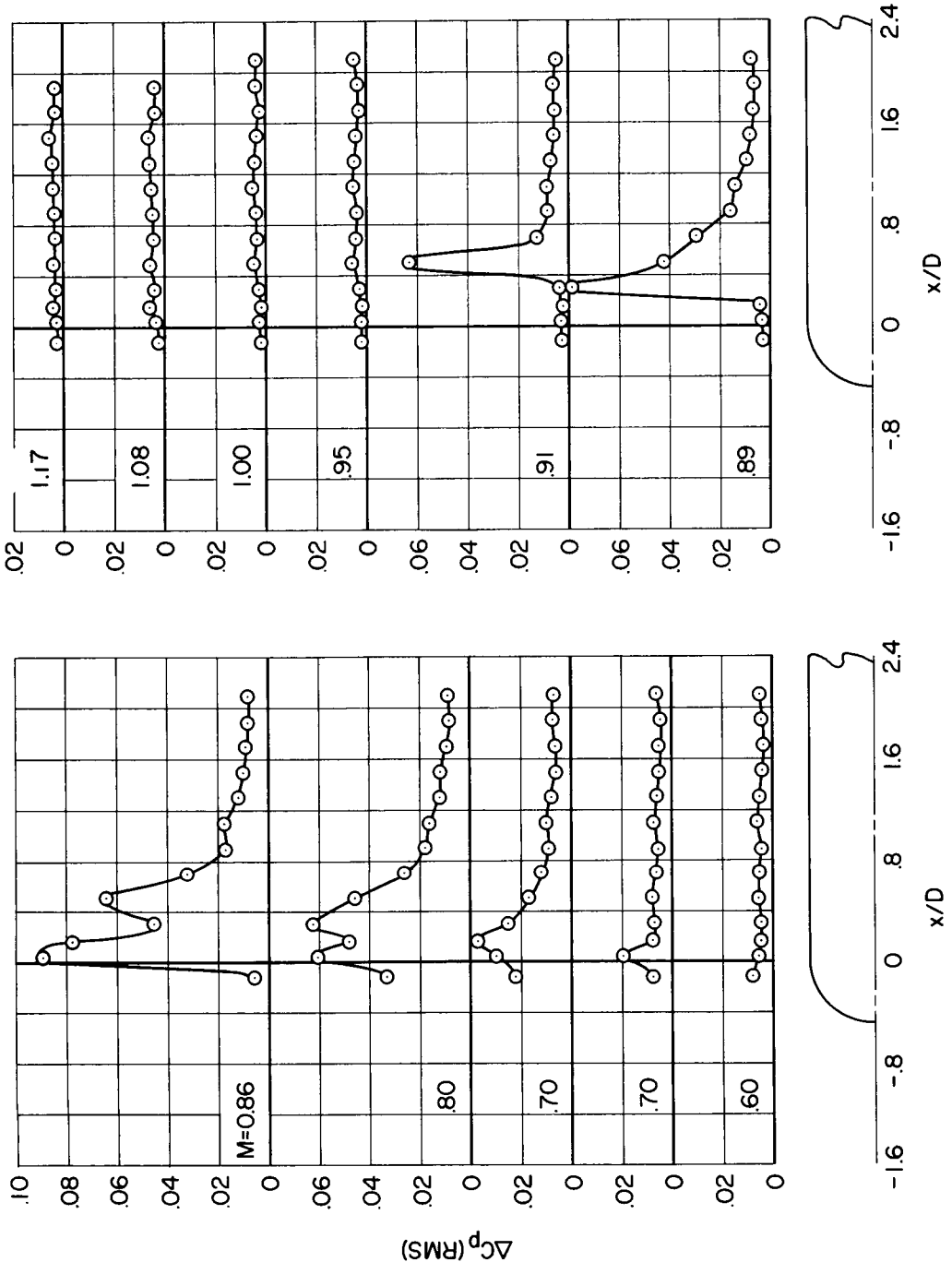

(b) $\alpha = 4^{\circ}$

Figure 10.- Continued.

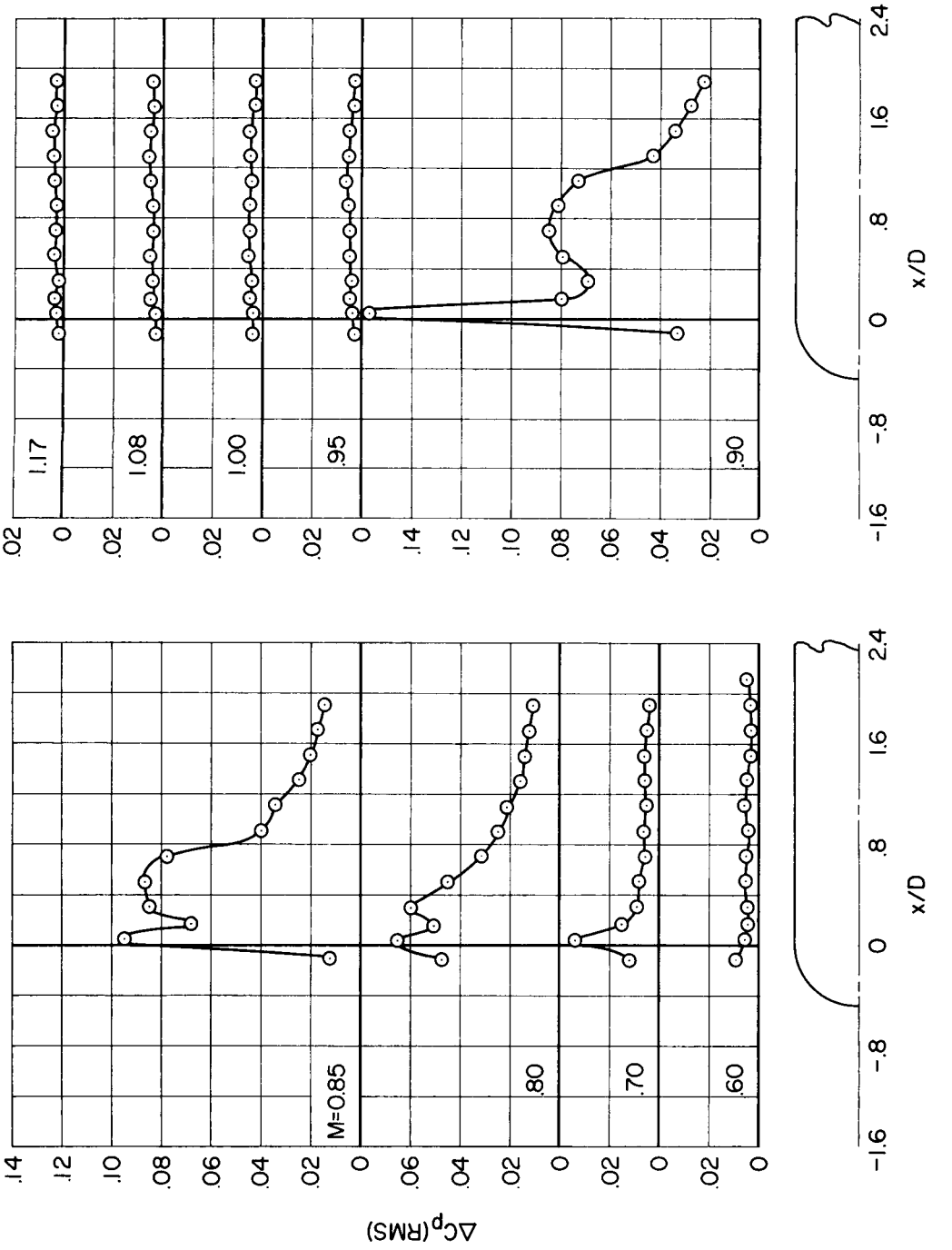

(c) $\alpha = 8^{\circ}$

Figure 10.- Concluded.

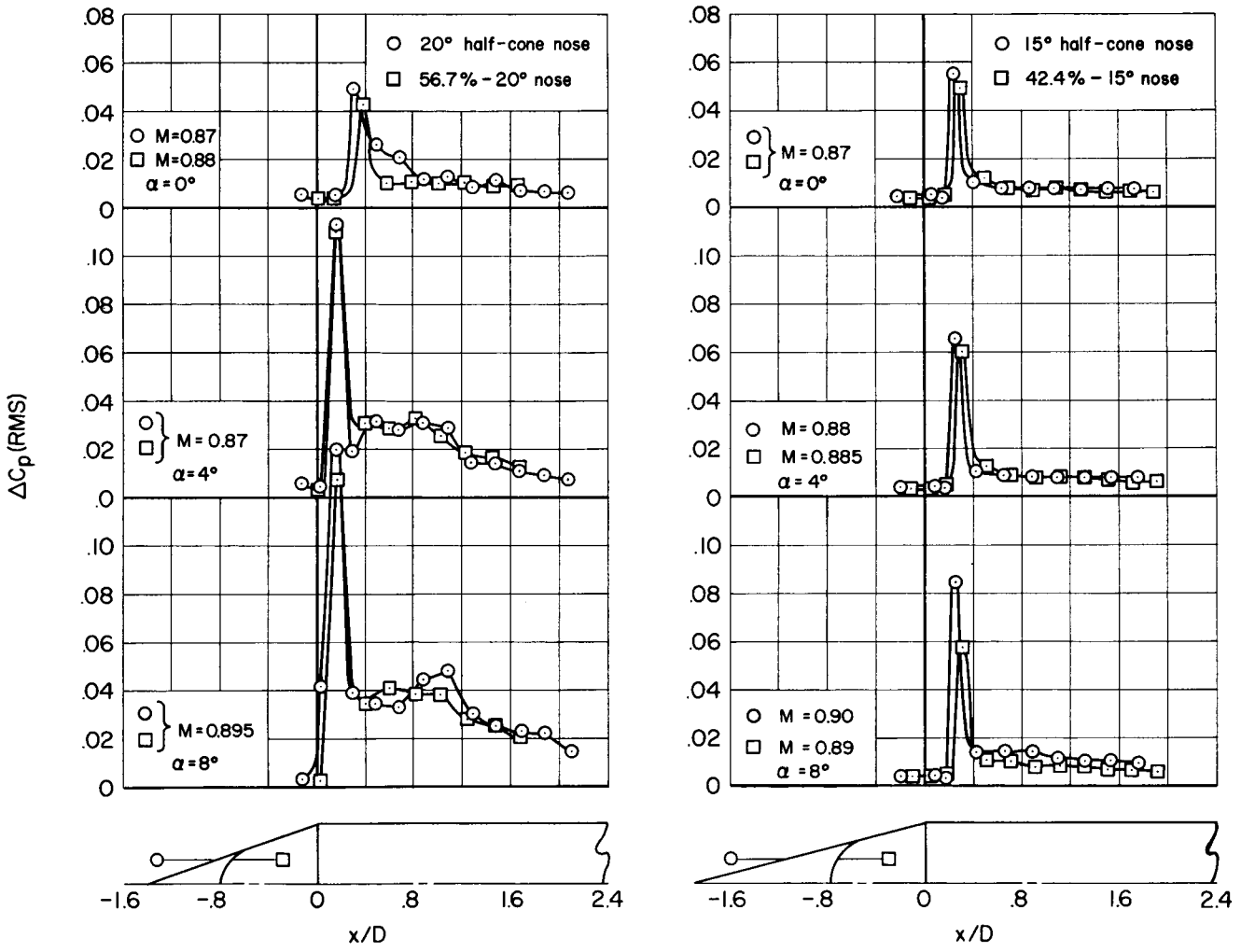

Figure 11.- Comparison of representative distributions of the pressure fluctuations showing the effects of cone angle and cone bluntness.

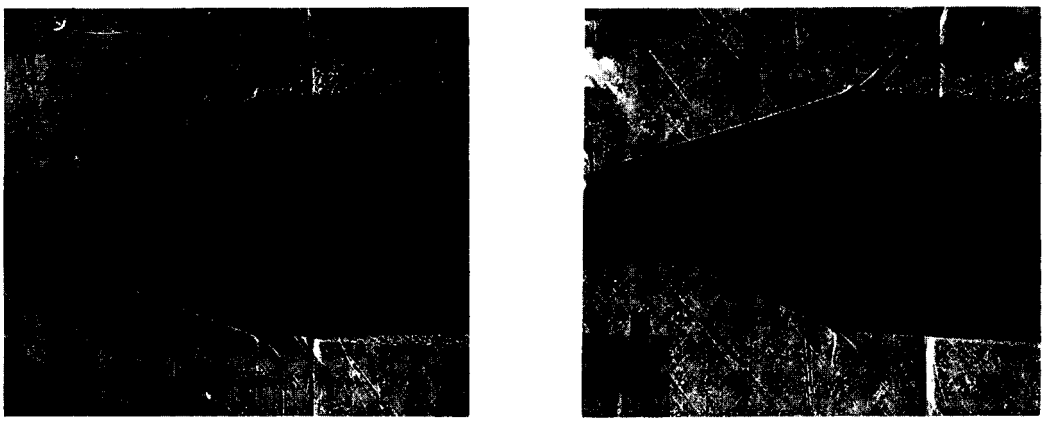

20° cone-cylinder model, $\frac{h}{H_{20}} = 1.$

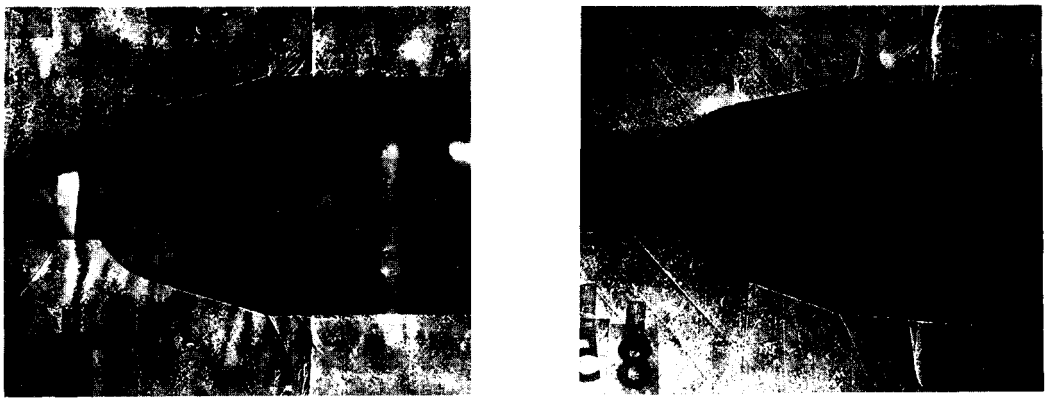

15° cone-cylinder model, $\frac{h}{H_{15}} = 0.424.$

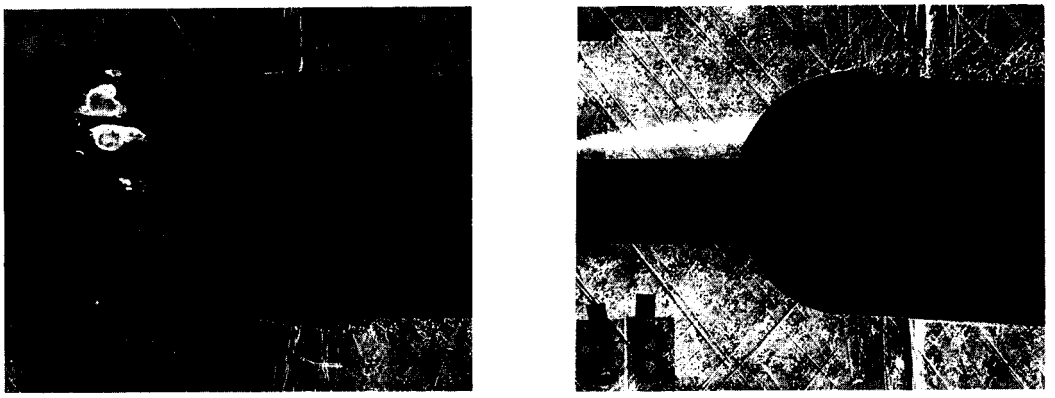

Hemisphere model

$M = 0.80, \alpha = 0^{\circ}$ $M = 0.85, \alpha = 4^{\circ}$

Figure 12.- Shadowgraph pictures showing the effect of some of the nose shapes on the flow.